Original article

Adsorption capacity of the biochar obtained from *Pinus patula* wood micro-gasification for the treatment of polluted water containing malachite green dye

A. Rubio-Clemente [a,b,c,1,]*, J. Gutiérrez [d], H. Henao [b], A.M. Melo [b], J.F. Pérez [d,3], E. Chica [b,2]

[a] *Facultad de Ingeniería, Tecnológico de Antioquia-Institución Universitaria TdeA, Calle 78b, No. 72A-220, Medellín 050034, Colombia*
[b] *Grupo de Energía Alternativa (GEA), Facultad de Ingeniería, Universidad de Antioquia, Calle 70, No 52-21, Medellín 050010, Colombia*
[c] *Facultad de Ingenierías, Universidad de Medellín, Cra. 87, No. 30-65, Medellín 050030, Colombia*
[d] *Grupo de Manejo Eficiente de la Energía (GIMEL), Facultad de Ingeniería, Universidad de Antioquia UdeA, Calle 70, No. 52-21, Medellín 050010, Colombia*

ABSTRACT

In this work, the adsorption capacity of the biochar obtained from *Pinus patula* biomass micro-gasification was studied using malachite green (MG) as the probe pollutant. For this purpose, the biomass type (wood pellets and chips) was selected to produce two kinds of biochar (BC). Afterwards, the effects of the adsorbent dose (6, 9 and 12 g/L), the solution pH (4, 7 and 10) and the BC particle size distribution (150–300, 300–450 and 450–600 μm) for the maximization of the MG retention by the selected BC were evaluated using a faced-centered central composite design, as response surface methodology. The results indicated that the BC derived from wood chips (BWC) exhibited a higher MG dye adsorption capacity than the BC obtained from the wood pellets (BWP) gasification under the same operating conditions after having reached the equilibrium. A second-order regression model was built for describing the MG adsorption behaviour by BWC under the considered experimental domain. The model, which was validated, resulted to be statistically significant and suitable to represent the MG adsorption by the studied BC with a p-value of 0.00 and a correlation coefficient (R^2) of 95.59%. Additionally, a three-dimensional response surface graph and a contour plot were utilized to analyze the interaction effects between the factors influencing the adsorption system and to discern the optimal operating conditions for the use of BWC. The maximal MG dye retention (99.70%) was found to be at an adsorbent dose, pH solution and a particle size distribution of 9.80 g/L, 10 and from 150 to 300 μm, respectively. Therefore, the BWC tested can be utilized for the treatment of water polluted with dyes, contributing to the establishment of a circular economy.

1. Introduction

Water is a natural resource that is essential for life. Every day, industries, agricultural activities and general population using water are growing in an exponential way, resulting in the pollution of this precious resource with toxic compounds (Kurniawan et al., xxxx), which can be bioaccumulated in the human body and produce several dangerous illnesses (Kosek et al., 2020). In recent decades, the majority of researches have been focused on the study of the so-called emerging contaminants, heavy metals, pesticides, dyes and other hazardous chemicals. The presence of these pollutants, particularly dyes, in aquatic ecosystems results in a considerable damage to the environment. In fact, dyes are toxic substances that lead to a high dissolved oxygen consumption in water, causing a negative impact (Tong et al., 2019). Additionally, dyes produce the coloration of water, limiting the activity of the photosynthetic organisms. For the particular case of malachite green (MG), which is a cationic triphenylmethane dye, it is extensively used in the fish farming and textile industries as an

* Corresponding author at: Facultad de Ingeniería, Tecnológico de Antioquia-Institución Universitaria TdeA, Calle 78b, No. 72A-220, Medellín 050034, Colombia.
E-mail address: ainhoarubioclem@gmail.com (A. Rubio-Clemente).
[1] ORCID ID: https://orcid.org/0000-0003-1527-260X
[2] ORCID ID: https://orcid.org/0000-0002-5043-6414
[3] ORCID ID: https://orcid.org/0000-0002-3811-4471

A. Rubio-Clemente, J. Gutiérrez, H. Henao et al.

antiprotozoal and antifungal product. Unfortunately, MG and leucomalachite green (a MG metabolite) can cause serious problems to human cells, especially to the immune and reproductive systems, due to their highly genotoxic and carcinogenic character (Stammati et al., 2005; Vyavahare et al., 2018; Mohamed et al., 2019).

Although the use of MG has not been authorized in the European Union, in the United States of America and in other countries, this toxic dye is still being commercialized in many countries around the world, specifically in least developed countries, because of its availability at a low cost and the multiple uses associated (Gwenzi et al., 2017). Additionally, among other dyes, MG is a substance resistant to degradation and may escape from water treatment facilities operating with traditional systems (e.g., coagulation-flocculation, chemical oxidation, sedimentation, filtration and disinfection), undergoing a limited alteration (Tkaczyk et al., 2020). Therefore, the implementation of efficient techniques is mandatory to avoid the presence of this and other toxic compounds within the aquatic environment and, subsequently, to protect living beings and human health (Rubio-Clemente et al., 2021, 2020). Different remediation methods, such as biological and electrochemical processes, have been applied to remove MG dye in water. Nevertheless, these technologies are often expensive, ineffective and time consuming. In this regard, adsorption is one of the most attractive techniques for eliminating pollutants in water (Jawad et al., 2017; de Farias et al., 2020; Hamad, 2021; Jawad et al., 2020; Jawad and Abdulhameed, 2020; Surip et al., 2020) and the use of biochar (BC), a carbon-rich solid by-product obtained from the biomass conversion process, has been considered as an attractive option for water decontamination (Zhang et al., 2020). BC, used as an adsorbing material, is characterized by the ease and sustainability of the control process, its effectiveness and the low-cost requirements (Nidheesh et al., 2020). Additionally, BC can be easily implemented in many rural communities inhabiting developing countries for the elimination of pollutants in water (Gwenzi et al., 2017).

The adsorption technique based on BC has been already employed for the treatment of effluents from the textile sector containing MG (Kayan et al., 2017; Rajabi et al., 2016; Mohamed et al., 2019; Tong et al., 2019). The referenced studies report that the utilization of biomass from several origins and the biochars (BCs) produced has advantages in the treatment of environmental matrices and in the management of waste. Nevertheless, information about the MG adsorption behaviour by the BC generated from the biomass micro-gasification process is limited in the literature. Indeed, from the authors' knowledge, no studies investigating the use of the BC generated from the micro-gasification of *Pinus patula* wood pellets (BWP) and chips (BWC) for the removal of MG in water have been reported nowadays.

In addition to the intrinsic characteristics of the adsorbing agent, it is important to note that the efficiency of the adsorption process depends on the correct choice of the operating factors, including the pH of the solution and the BC particle size and dose. For this purpose, optimization techniques must be used and one-factor-at-a-time (OFAT) methodology has been commonly applied. However, because of OFAT technique does not allow to evaluate simultaneously the effect of the entire set of parameters considered to influence the response variable(s) within the experimental domain (i.e., on the removal of the pollutant of interest), the response surface methodology (RSM) has been recently positioned as an alternative optimization technique able to overcome the limitations ascribed to the former one (Bezerra et al., 2019; Montgomery, 2020). Moreover, the application of RSM results in a low number of runs needed to evaluate interactions of multiple parameters, leading to the reduction of the operation time and associated costs (Jawad et al., 2017; Manojkumar et al., xxxx;

Jawad et al., 2020; Jawad and Abdulhameed, 2020; Surip et al., 2020).

Under this scenario, this research is focused on studying the adsorption of MG dye in water using two different eco-friendly BCs produced from the micro-gasification of *Pinus patula* wood pellets and chips (BWP and BWC, respectively). The effect of the operating conditions, including the adsorbent dose (BC-D) (6, 9 and 12 g/L), the solution pH (4, 7 and 10) and the BC particle size distribution (BC-PSD) (150–300, 300–450 and 450–600 μm), on the BC adsorption capacity is analyzed. RSM, through a face-centered central composite design of experiments (CCD), is used to optimize the treatment system aiming at maximizing the MG dye removal in order to demonstrate the important role played by a solid waste for the remediation of water, the establishment of a circular economy and, subsequently, the contribution to the sustainable development.

2. Methods and materials

2.1. BC generation, characterization and treatment

The BCs used in this work were produced from the gasification of patula pine (*Pinus patula*) wood in the form of pellets (WP) and chips (WC). This species was selected because of the harvested area ($\sim$38500 ha), annual yield ($\sim$20 m^3/ha per year) and the $\sim$13-year cutting cycle, along with its dendro-energy potential in Colombia (Pérez et al., 2019). WP and WC were used due to they are considered as the most common worldwide wood presentation for the production of energy (Hubbard, 2015). The pellets were 8-mm diameter, had a length from 10 to 15 mm and were provided by a local sawmill placed in Medellín, Colombia. In turn, the chips were produced by the Bandit 95XP equipment and had a particle size that ranged from 4 to 20 mm. It is highlighted that the oxidation stability during the gasification process is influenced by the particle size range (Lenis and Pérez, 2014).

Gasification was performed in a top-lit updraft (TLUD) reactor, which was operated at an atmospheric pressure, in order to obtain combustible gas (composed of hydrogen, methane, carbon monoxide, a small amount of hydrocarbons and other non-combustible gases, including carbon dioxide and nitrogen) and BC. The generated BCs were used as bio-adsorbents for the treatment of water polluted with MG due to their high adsorption capacities, among other physicochemical properties (Nidheesh et al., 2020).

The TLUD reactor, with a height of 0.28 m and 0.16 m of inner diameter, had a cylindrical shape. The reactor used a line of atmospheric air as the gasification agent, which was provided by a reciprocating compressor (up to 254 L/min, 3000 rpm and 2.60 kW) with a volumetric vessel. The line had a rotameter and a manometer to control the air flow and the pressure, respectively. A fixed air flow (V_{air}) equal to 146 ± 4.35 L/min was used for the studied biomasses. For monitoring the temperature inside the gasification bed, 5K-type thermocouples (±1 °C) were utilized. The thermocouples were separated every 0.04 m longitudinally along the reactor. Additionally, the reactor had a National Instruments USB-6001 acquisition card (DAQ) and a program developed in the LabView®software that were used for the control and acquisition of data. Within the reactor, the fresh biomasses were ignited at the top; therefore, the reaction front at a temperature of approximately 700 °C dropped to the reactor grate on the bottom. The gasification parameters associated with the BC production reached a biomass-air equivalence ratio (F_r) of 1.52 ± 0.19 for WP and 1.85 ± 0.25 for WC; the specific biomass consumption rate (m_{bms}) ranged from 125.33 (±15.48) kg/h/m^2 for WP to 145.39 (±19.72) kg/h/m^2 for WC. Furthermore, the BC yields (Y_{char}) reached for WP and WC were 12.12 (±1.19) wt% and 10.82 (±1.24) wt%,

A. Rubio-Clemente, J. Gutiérrez, H. Henao et al.

respectively. The analyses related to the gasification process of the biomass samples (WP and WC) and the experimental setup are described in detail by Gutiérrez et al. (2021).

The produced BCs were characterized through elemental and proximate analyses. From the latter one, the volatile material (VM), the ash content and the fixed carbon content (AC and FC, respectively) were determined. For this purpose, a TGA Q50 equipment (TA Instruments, USA) was used following the modified ASTM-D 5142-04 method, as proposed by Medic et al. (2010).

In turn, the BC ultimate analysis, which included the determination of hydrogen (H), carbon (C), oxygen (O), nitrogen (N) and sulfur (S) contents, was conducted as reported in ASTM D5373-08 method (Protásio et al., 2013) using a Leco Truspec micro (Leco®, USA). On the other hand, the specific surface area was quantified based on the N_2 adsorption/desorption with the Brunauer-Emmett-Teller (BET) N_2 sorption technique using an ASAP 2020 kit (Micromeritics Instrument Corp., USA). Furthermore, the changes of the functional groups contained on the wood biomass surface before and after gasification were qualitatively analyzed using a Fourier Transform Infrared spectroscopy (FTIR) (Qian et al., 2013). For a qualitative FTIR, a potassium bromide (KBr) pellet was prepared at 2 wt% of sample (wood or BC). The baselines of the FTIR spectra were superimposed for obtaining a qualitative comparison. An IRAffinity-1 with a detector operated in the 4000–400 cm^{-1} wave number range (Shimadzu, Japan) was used for the FTIR analysis. In turn, the pore volume was determined through the Barrett, Joyner and Halenda method (BJH). The BC bulk density (ρ) was also measured. The NTC 5167 standard (ICONTEC, 2011) was used to determine the BC cation exchange capacity (CEC) and pH. Additionally, the fiber content (%wt), in terms of lignin, cellulose and hemicellulose, was determined following the procedure and methodology proposed by Van Soest et al. (1991). The higher heating value (HHV) was also analyzed (Gutiérrez et al., 2021).

In Fig. 1, both of the biomasses used (WP and WC) and their respective BCs (BWP and BWC) are represented. It is important to mention that BWP demonstrated a considerable mechanical resistance when handled compared to that one obtained in BWC.

After having been produced and cool-down, both types of BCs were finely crushed and sieved to obtain three different particle size fractions (150–300 μm [fine], 300–450 μm [medium] and 450–600 μm [coarse]). Subsequently, the BCs were stored at a room temperature in plastic bags with a zipper closure up to analysis and experimentation.

2.2. Chemicals and reagents

For the BC physicochemical characterization, potassium bromide (KBr, >99%) was used in the FTIR test. In turn, 100 mL of acid and neutral detergent solutions (>99%) were used in the determination of the contents of neutral and acid detergent fibers. The analysis of lignin in acid detergent was carried out using 15 mL of a 72% sulfuric acid (H_2SO_4, 96%) solution. Ammonium acetate ($CH_3CO_2NH_4$, >97%), ethanol (C_2H_5OH, 95%), sodium chloride (NaCl, >99%), formaldehyde (CH_2O, 37%), 1,10-phenolphthalein ($C_{12}H_8N_2$, 99%) and sodium hydroxide (NaOH, 99%) were used to determine the CEC of the tested BCs. Regarding the ultimate and BET analyses, helium (He, 99.99%) and nitrogen (N_2, 99.99%) were used at a flow rate of 40 psi; both gases were 5.0 grade. N_2, at a flow rate of 100 mL/min, was also used to discern the VM of the studied BCs; besides, He was also used for the proximate analysis and the determination of N, C, O, H and S contents. The supplier of these gases was Messer (Colombia). In turn, the AC was determined using atmospheric air at a flow rate of 100 mL/min.

The probe compound used for monitoring the adsorption capacity of the studied BCs was malachite green dye (99%), which was purchased from Carlo Erba (Italy). Additionally, NaOH ($\geqslant$98%) and nitric acid (HNO_3, 65%) were purchased from Macron Fine Chemicals (Mexico) and Merck (Germany), respectively, and were used to adjust the pH of the water to be treated up to the desired pH value. These chemicals were reactant grade and were used without further purification.

2.3. Dye adsorption experiments

The BCs produced from the micro-gasification process of WP and WC were separately evaluated as adsorbing agents of MG contained in water. For this purpose, batch experiments were carried out immersing into a 0.6 L glass tank a known amount of the tested BC after having been crushed and sieved, so that different BC particle sizes ranges were obtained (150–300 μm, 300–450 μm and 450–600 μm). The glass tank contained 300 mL of tap water, which was spiked with a 1000 mg/L MG solution until a MG concentration of 50 mg/L was obtained. The amounts of BC used were 1.80, 2.70 and 3.60 g, which were equivalent to a BC-D of 6, 9 and 12 g/L, respectively. Then, few drops of 1N NaOH or 1N HNO_3 solutions were added to reach the desired pH (4, 7 and 10). The aqueous solution was stirred with a magnetic stirrer and a stir bar. Studies were conducted in triplicate. The average results were recorded along with the standard deviations, with the exception of the optimization experiments where only the average results for each treatment were reported for calculation reasons. At 1, 2, 3, 4, 5, 10, 15, 30 and 60 min of treatment time, a known volume of the dye solution with BC was withdrawn during the preliminary experiments. For the optimization procedure, aliquots at 5 min of treatment were collected. To separate the residual BC in the whole set of aliquots, a nylon syringe filter of 0.45 μm was used.

2.4. Analysis of the BC adsorption capacity

The MG adsorption on the tested BCs was analyzed using visible spectrophotometry. For this purpose, the visible spectrum of the probe dye was scanned in a Spectronic 200 visible spectrophotometer (Thermo Scientific, USA). The maximum absorption wavelength was fixed at 622 nm. Afterwards, a calibration curve with a correlation coefficient (R^2) of 99.95% was constructed to determine the analyte concentration in water. Finally, the removal capacity of the tested BCs throughout the time of treatment was calculated as described in Eq. (1), where C_0 and C_t refer to the MG initial and final concentrations (mg/L), respectively.

$$Removal = \frac{C_0 - C_t}{C_0} 100\% \tag{1}$$

2.5. Design of experiments

The effect of the operating conditions, including the adsorbent dose (6, 9 and 12 g/L), pH of the solution (4, 7 and 10) and the BC particle size distribution (150–300, 300–450 and 450–600 μm), on the adsorption capacity of the selected BC from the tested adsorbing materials was investigated using RSM, particularly a face-centered CCD. The above-mentioned levels were selected according to the reported information concerning the removal of dyes in water. Additionally, with regard to the solution pH, covering the ranges of pH values commonly found in surface water was considered in order to avoid an excessive reduction or rise of this parameter during water treatment processes. This aspect will allow to further reduce the intrinsic low operating costs associated, favoring the scaling-up of the studied technology.

The list of the independent variables, or factors, with their symbols (x_1, x_2, x_3) and levels are presented in Table 1. The factors were
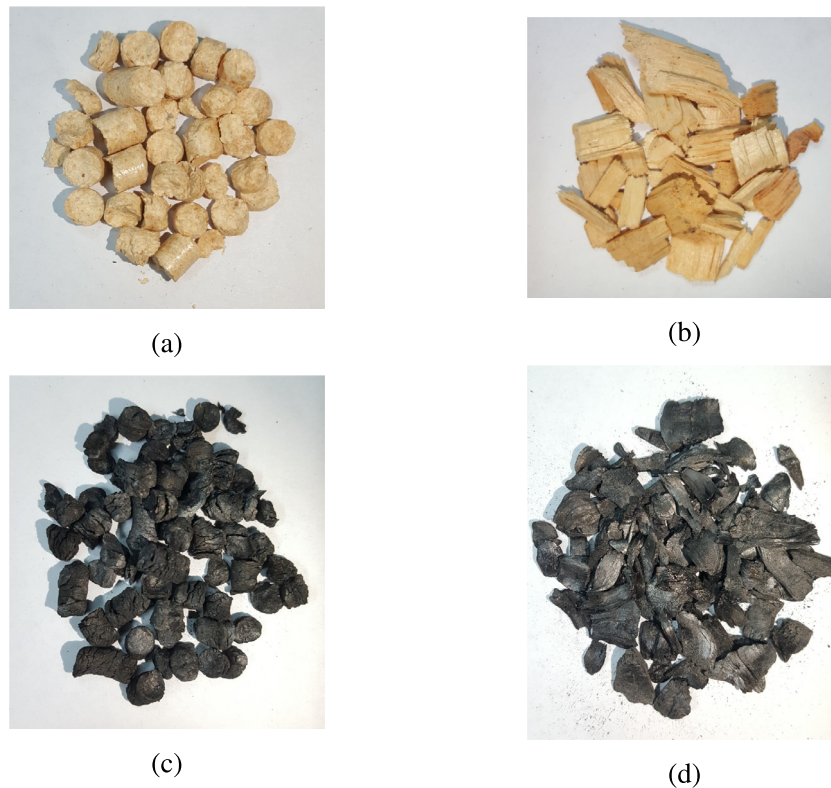
A. Rubio-Clemente, J. Gutiérrez, H. Henao et al.

(a)

(b)

(c)

(d)

Fig. 1. Biomass feedstocks and derived BCs. a) WP, b) WC, c) BWP and d) BWC. Operating conditions: V_{air} = 146 L/min; F_r = 1.52 for BWP and 1.85 for BWC; m_{bms} = 125.33 kg/h/m^2 for BWP and 145.39 kg/h/m^2 for BWC; Y_{char} = 12.12 wt% for BWP and 10.82 wt% for BWC.

Table 1
Factors and levels used in the face-centered CCD.

Independent factor (unit)	Real values of coded levels			Symbol
	−1	0	+1	
Biochar dose, BC-D (g/L)	6	9	12	x_1
pH of the solution, pH	4	7	10	x_2
Biochar particle size distribution, BC-PSD (μm)	150–300	300–450	450–600	x_3

−1, 0 and +1: Factor at a low, medium and a high level, respectively.

studied and varied within 3 levels: a) a high level, represented as (+1); b) a low level, referred as (-1); and c) a middle point, expressed as (0). The response variable (y) was the percentage of MG removed in water by the BC. The response was intended to be maximized.

To fit the obtained experimental results, a second-order regression model represented by Eq. (2) was chosen. This model describes the main and quadratic effects, as well as the interactions of the selected factors (x_1, x_2, x_3) influencing the response variable (i.e., the removal percentage of MG). It must be noted that interaction occurs when the effect of one independent factor on the response is dependent on the level of another independent parameter (Montgomery, 2020).

$$y = \beta_0 + \beta_1 x_1 + \beta_2 x_2 + \beta_3 x_3 + \beta_{12} x_1 x_2 + \beta_{13} x_1 x_3 + \beta_{23} x_2 x_3$$
$$+ \beta_{11} x_1^2 + \beta_{22} x_2^2 + \beta_{33} x_3^2 \qquad (2)$$

where, y is the predicted response concerning the amount of MG adsorbed on the biochar, β_0 is a constant value of the regression model; β_1, β_2 and β_3 are the linear coefficients, corresponding to the main effects of the considered factors; β_{12}, β_{13} and β_{23} are the cross-product coefficients representing the interaction effects.

Finally, β_{11}, β_{22} and β_{33} are the quadratic coefficients of the parameters considered to affect the adsorption system.

According to the CCD experimental matrix, a set of 17 treatments was generated. The runs were randomly executed in order to avoid bias and dependence of the observations. Each treatment was placed in a different glass tank.

2.6. Data treatment

The statistical software Statgraphics Centurion XVII$^®$(StatPoint Technologies, USA) was used to analyze the experimental data. In order to assess the significance and adequacy of the second-order regression model built, an analysis of variance (ANOVA) was performed considering a p-value lower than 0.05. The fit of the quadratic regression model was evaluated through the examination of R^2 and the correlation coefficient adjusted by the degrees of freedom (R_{adj}^2) (Montgomery, 2020). Additionally, the second-order regression model was validated and its significance and adequacy were checked, including the normality, homoscedasticity and independency assumptions. Finally, the optimal values of the factors considered to influence the adsorption capacity of the tested BC on the MG retention were estimated using a response surface analysis,

A. Rubio-Clemente, J. Gutiérrez, H. Henao et al.

taking into account the maximization of the removal of MG (%) according to Eq. (1).

3. Results and discussion

3.1. Selection of the BC type and the residence time

Once the studied BCs were generated, they were characterized. The physicochemical properties of the BCs evaluated are compiled in Table 2.

In Fig. 2, the adsorption of MG (50 mg/L) on BWP and BWC throughout 60 min of treatment time is shown. Clearly, it can be observed that BWC is more effective in adsorbing MG in comparison with BWP under the evaluated experimental domain. In fact, after 5 min of residence time, the MG removal values in water by BWP (Fig. 2a) and BWC (Fig. 2b) were 39.30% and 60.10%, respectively, at a solution pH and temperature of 4 and 24 °C, respectively. Therefore, it is demonstrated the importance of the type of the biomass used during the gasification process for obtaining the BC to be applied in water treatment, keeping fixed the other variables (BC-PSD and BC-D equal to 150–300 μm and 6 g/L, respectively) with respect to the time at which the adsorption equilibrium is reached.

As observed in Table 2 and reported by Gutiérrez et al. (2021), the BCs tested showed differences in the physicochemical characteristics analyzed. As a matter of fact, concerning the surface area, BWC exhibited a lower value compared to the surface area obtained for BWP. As it is widely known, the surface area plays an important role in the adsorption capacity of an adsorbing material (Tong et al., 2019). However, in the current case, although the dose of the BC was fixed for both types of BCs, due to BWC has associated a lower density in comparison with BWP, the number of particles prompted to react with MG was higher for the former one and, consequently, the amount of active sites available for the adsorption of MG was increased. This would be the reason why the maximal adsorption was obtained for BWC keeping fixed the other variables.

The time-dependence of the adsorption capacity of the BCs used is also shown in Fig. 2, obtaining the adsorption equilibrium about 5 and 30 min for BWC and BWP, respectively. In the experimental test where BWP was used at a pH, adsorbing agent dose and particle size distribution values of 10, 6 g/L (equivalent to a BC amount of 1.80 g) and 150–300 μm, respectively, the MG removal percentage increased from 66.90% at 5 min of residence time to 81.60% after 10 min of treatment. The removal capacity of 84.60% was observed at the equilibrium point (30 min). Under the above-mentioned operating conditions, the maximal removal of MG dye by BWC was 85.90% after 5 min of residence time. This indicated that the adsorption capacity of the probe dye is increased at a lower time of treatment when BWC is used, leading to a higher efficiency of BWC compared to BWP.

Concerning the MG uptake capacities of both of the BCs used, two different steps can be observed. In the former one, a sharp adsorption of MG is observed as the residence time is increased. With regard to the second adsorption step, the MG uptake by the tested BCs slows down. This step represents the time at which the equilibrium for complete saturation of the BCs is achieved, since the amount of MG retained by the BCs does not change significantly. The equilibrium for the BCs tested was found at 5 min and 30 min for BWC and BWP, respectively.

Several authors in the literature have also observed these two steps (Jawad et al., 2017; Abukhadra et al., 2019; Jawad et al., 2020; Jawad and Abdulhameed, 2020; Liu et al., 2020; Surip et al., 2020). The highest removal rate during the initial stage can be explained from the vast number of free active sites that are

Table 2
Physicochemical characteristics of BWC and BWP. Operating conditions: V_{air} = 146 L/min; F_r = 1.52 for BWP and 1.85 for BWC; m_{bms} = 125.33 kg/h/m^2 for BWP and 145.39 kg/h/m^2 for BWC; Y_{char} = 12.12 wt% for BWP and 10.82 wt% for BWC.

Property (units)	BC type	
	BWC	BWP
VM (wt%)	24.36	20.59
FC (wt%)	72.90	77.49
AC (wt%)	2.74	1.92
C (wt%)	97.06	97.94
H (wt%)	0.85	0.97
O (wt%)	1.66	0.90
N (wt%)	0.43	0.19
O/C	0.01	0.01
H/C	0.11	0.12
HHV (MJ/kg)	28.36	29.25
Lignin (wt%)	77.00	86.00
Cellulose (wt%)	1.10	1.69
Hemicellulose (wt%)	1.51	1.04
pH	9.10	8.80
BET (m^2/g)	233.56	367.33
CEC (meq/100 g)	22.60	21.70
ρ (kg/m^3)	91.05	236.28

available. Then, as MG is retained by BC, the number of free active sites is decreased until the equilibrium is reached. Finally, the saturation of the adsorbing material is achieved.

Therefore, due to the BWC maximal adsorption capacity under the experimental conditions tested, BWC was characterized in detail and used in further experiments to discern the effect of the independent parameters listed in Table 1 on the BWC adsorption capacity in water, and to optimize the operating conditions aiming at the MG removal maximization.

3.2. BWC characterization

The morphology of the BWC was analyzed using scanning electron microscopy (SEM). For this purpose, a JEOL JSM-6490 microscope (Jeol Ltd., Japan) operating at an acceleration voltage of 20 kV was utilized. The samples were covered by a gold film before being introduced to the equipment. As observed in Fig. 3a, the *Pinus patula* WC had a strongly solid and fibrous structure, which was characterized by the lack of pores unlike the derived BC, where several pore sizes were formed during the biomass gasification process (Fig. 3b). The presence of a porous structure in the BC may be linked to the pyro-combustion process due to the cellulose and hemicellulose degradation. However, when a more complete destruction of the initial structure occurs under a limited oxygen structure, a higher number of pores is formed (Gutiérrez et al., 2021); which is related to the high combustion temperature values used (Wu et al., 2020).

When the biomass is micro-gasified, the pores are opened and the internal diameters are widened; as a consequence, the surface area (BET) is increased in the BC compared to the raw biomass due to the VM release (González and Pérez, 2019). That is the reason why the BET values of BWC were significantly different compared to the BET values of WC (Gutiérrez et al., 2021).

A FTIR analysis was also conducted for WC, as mentioned previously. In Fig. 4, the FTIR spectra of the BCs and the raw biomass were illustrated. In contrast to the FTIR spectrum of the raw biomass, in the derived BC several functional groups were lost, mainly those ones related to the OH and CH bands, which can be supported by the BC aromaticity index (0.75) compared to that of the raw biomass (0.16) (Gutiérrez et al., 2021). After the biomass gasification, a portion of the content of water and VM is released, leading to the decrease in the derived BC of the peaks in the range 3700–3000 cm^{-1}, which corresponds to the hydroxyl and phenolic
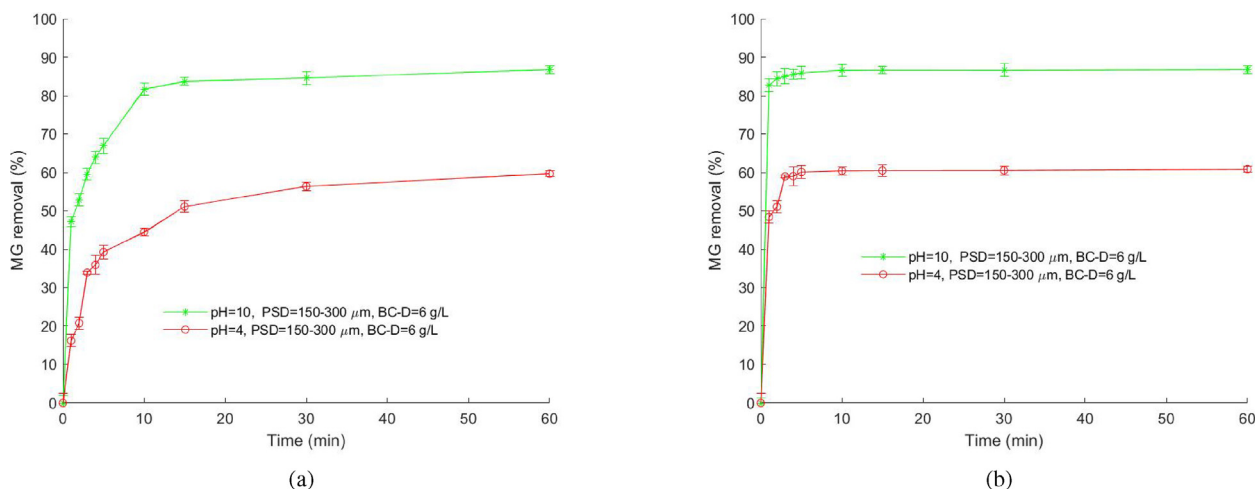
A. Rubio-Clemente, J. Gutiérrez, H. Henao et al.

(a)   (b)

Fig. 2. MG adsorption vs. time by a) BWP and b) BWC. Operating conditions: $[MG]_0$ = 50 mg/L; pH = 4 and 10; BC-D = 6 g/L; BC-PSD = 150–300 μm; time = 60 min.
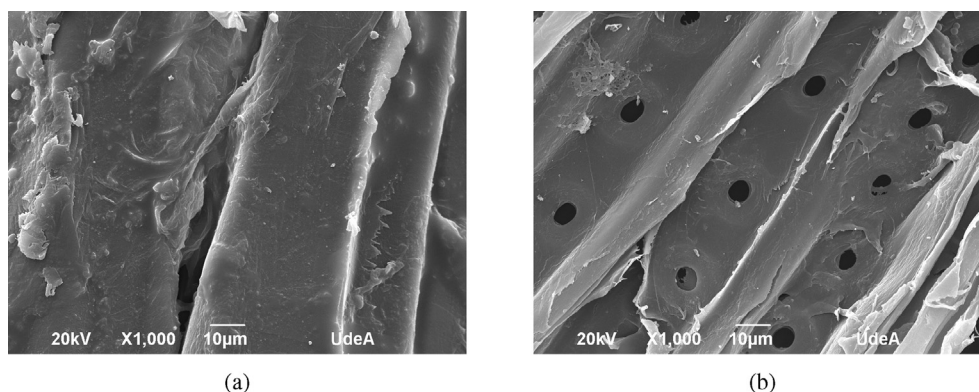

(a)   (b)

Fig. 3. SEM images X1000 for a) WC and b) BWC. Operating conditions: V_{air} = 146 L/min; F_r = 1.85; m_{bms} = 145.39 kg/h/m^2; Y_{char} = 10.82 wt%.
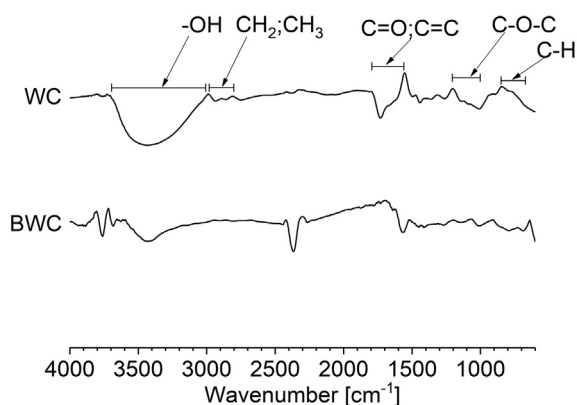

Fig. 4. FTIR spectra for WC and BWC. Operating conditions: V_{air} = 146 L/min; F_r = 1.85; m_{bms} = 145.39 kg/h/m^2; Y_{char} = 10.82 wt%.

groups (-OH), water molecules and -OH stretching (Qian et al., 2013). Additionally, during the biomass gasification, hemicellulose and cellulose contents are thermally decomposed; therefore, the peaks in the range 2980–2800 cm^{-1}, which is related to the CH$_2$ and CH$_3$ aliphatic groups stretching, were not observed in BWC, as well as the peaks within the range 1800–1600 cm^{-1}; which may be attributed to the lignin and hemicellulose contents, and the existence of water, alkyl functional groups and oxygenated hydrocarbons, resulting in the C=O ring stretching, C=C aromatic

ring vibrations and the flexural modes in the -OH plane (Jindo et al., 2014; Díez and Pérez, 2019). Furthermore, in the raw biomass, C-O-C bonds were stretched because of the hemicellulose and cellulose contents, resulting in the occurrence of peaks in the range 1200–1000 cm^{-1} (Qian et al., 2013). However, after gasification, an aromatic structure was found in the derived BC due to the C=C ring stretching and the C-C aromatic deformation (Díez and Pérez, 2019), leading to the loss of the peak located at 1520 cm^{-1} and the peaks between 850 cm^{-1} and 650 cm^{-1}, respectively.

The disappearance of several functional groups after the thermochemical decomposition of the biomass was also reported by Wu et al. (2020). In turn, Lou and coworkers (2016) reported that an increase in the BC porosity after the biomass combustion led to a higher surface area and, subsequently, a better pollutant adsorption was found. This might probably due to the pore-filling effect with the toxic molecules (Lou et al., 2016).

3.3. Influence of the operating conditions on the BWC adsorbance capacity

To discern the effect of the operating conditions considered in the current study (i.e., pH, BC-D and BC-PSD), as well as their significance on the BWC adsorption capacity, a RSM based on a CCD was used. In Table 3, the design matrix representing the treatments that were randomly executed is displayed. After running the trials listed in Table 3, an ANOVA was carried out to construct a second-order regression model able to represent the MG dye adsorption

Table 3
Face-centered CCD matrix and experimental data for the removal of MG by BWC. Operating conditions: $[MG]_0$ = 50 mg/L; BC-D = 6–12 g/L; solution pH = 4–10; BC-PSD = 225–525 μm; time = 5 min.

Run	Factor			MG removal (%)	
	Biochar dose, BC-D (g/L), x_1	pH of the solution, pH, x_2	Biochar particle size distribution, BC-PSD (μm), x_3	Experimental data	Predicted data
1	6	4	225	60.10	57.14
2	12	4	225	61.50	62.08
3	6	10	225	85.90	88.16
4	12	10	225	91.30	93.10
5	6	4	525	40.60	39.86
6	12	4	525	49.80	44.80
7	6	10	525	81.10	81.08
8	12	10	525	85.30	86.02
9	6	7	375	65.10	66.56
10	12	7	375	69.60	71.50
11	9	4	375	49.00	55.68
12	9	10	375	98.00	91.80
13	9	7	225	79.00	79.83
14	9	7	525	60.10	67.65
15	9	7	375	75.20	73.74
16	9	7	375	78.40	73.74
17	9	7	375	76.50	73.74

capacity of the selected BC. In the ANOVA, the main effects of the studied parameters, as well as the interaction and the quadratic effects were included. It is important to note that ANOVA is a powerful tool that describes the significance of the terms influencing the system to be optimized (Montgomery, 2020); in the current case, the MG removal under the experimental domain considered here.

In Table 4, the results from the ANOVA are compiled. Based on the associated p-values, all the 3 factors evaluated were found to be statistically significant, as well as the interaction effect between the pH of the water to be treated and the BC-PSD, since they have p-values associated lower than 0.05, being the factor related to the pH of the solution the most significant one. The p-value of the quadratic effect of the BC-D was also lower than 0.05; therefore, it was considered as a statistically significant one.

In the Pareto chart (Fig. 5), the magnitude and the positive or negative influence of the mentioned effects are illustrated. In the chart, the effect surpassing the vertical line can be considered as a significant one from a statistical point of view. As observed, the pH of the solution was the main parameter affecting positively the adsorption capacity of the studied BC. This effect was followed by the BC-PSD, which in this case develops a negative role. Additionally, the BC-D was observed to influence the MG retention in a negative way but to a lesser extent in comparison with the pH of the polluted water. The quadratic effect concerning the BC-D was also negatively significant. Finally, the pH-PSD interaction affected the system positively.

In Fig. 6, the main effects of the considered factors are represented. It can be observed the positive effect developed by the pH of the solution in the adsorption system, as well as the main effect concerning the BC-D. Nevertheless, as observed in the figure, beyond the central point regarding the dose of the adsorbing material, an incipient curvature is depicted. This indicates that the quadratic effect ascribed to the BC-D must be considered in the constructed regression model representing the removal percentage of MG in water. Additionally, in Fig. 6, the negative effect exerted by the BC-PSD can be observed, since the removal of MG by the tested BC is decreased as the PSD used is increased.

3.3.1. Effect of the pH solution

The pH is a crucial factor when evaluating the adsorption capacity of any material. Indeed, the solution pH resulted to be the most significant factor (p-value equal to $0.08x10^{-2}$) among the parameters considered to influence the MG adsorption capacity by BWC.

The pH has a significant impact on the speciation of the pollutant in water and on the adsorption capacity of the BC used for treating the water pollution. Furthermore, the pH of the adsorbent is involved in the BC surface characteristics and, subsequently, in the adsorption efficiency of the probe dye by the adsorbing material.

In the current case, the BWC pH was 9.10. Additionally, the MG pK_{a1} and pK_{a2} values were 6.90 and 10.30, respectively. It is important to note that the pK_a stands for the chemical species the dye is found in water regarding the solution pH; i.e., at a $pH_{solution}$ < pK_{a2}, MG is mainly found in the ionized form; that is, MG cationic forms are abundant in the solution; whereas at a $pH_{solution}$ > pk_{a2}, MG is neutrally charged.

Here, the influence of the solution pH was evaluated in the range from 4 to 10. It was observed an increment in the MG adsorption by BWC as the pH of the solution was increased from 4 to 10, obtaining the maximal retention of MG dye at a pH value of 10 after 5 min of residence time. Therefore, it was concluded that the MG uptake was favored in an aqueous solution at a basic pH. This can be explained from the pH of the water solution and the pKa values of the probe dye. Since the attraction between the electronegatively charged BC and MG, which is charged positively, is promoted at a solution pH of 10, due to BWC has hydroxides ions (OH^-). Considering the MG structure, at a $pH_{solution}$ < pK_{a2}, it becomes a cationic dye, which can be adsorbed on the BC surface whose functional groups are negatively charged, as mentioned above. However, at a $pH_{solution}$ < pK_{a1}, although a higher amount of MG is charged positively in the aqueous solution, the negative charges in the BWC surface start to be reduced and protons (H^+) start to appear in the solution. Thus, H^+ and the MG cationic forms compete for the BC active sites as the pH of the solution is decreased, especially below the MG pK_{a1}.

Basic conditions in the water to be treated were also achieved as the optimal ones by Abukhadra et al. (2019). The referenced authors synthetized a novel hybrid material decorating diatomite skeletons by Ni/NiO nanoparticles and found the highest MG adsorption at a pH value of 8. Liu and coworkers (2020) also found basic conditions when evaluating the uptake of MG (Liu et al., 2020). Basic conditions were also observed for the adsorption of methylene blue (MB) cationic dye by several types of adsorbing materials, including mesoporous activated carbons from bamboo chips using KOH-assisted thermal activation (Jawad and Abdulhameed, 2020) and from corn cob residue via microwave-assisted H_3PO_4 activation (Jawad et al., 2020). Similar results were

Table 4
ANOVA of the second-order regression model representing the MG removal (%) using BWC. Operating conditions: $[MG]_0$ = 50 mg/L; BC-D = 6–12 g/L; solution pH = 4–10; BC-PSD = 225–525 μm; time = 5 min.

Source	DF	SS	MS	F-ratio	P-value
A:BC-D, x_1	1	61.01	61.01	23.56	3.99×10^{-2}
B:pH, $x2$	1	3261.64	3261.64	1259.32	0.08×10^{-2}
C:BC-PSD, x_3	1	370.88	370.88	143.20	0.69×10^{-2}
AA	1	91.46	91.46	35.31	2.72×10^{-2}
BC	1	52.02	52.02	20.08	4.64×10^{-2}
Lack-of-fit	9	216.29	24.03	9.28	1.01×10^{-1}
Pure error	2	5.18	2.59		
Total (corr.)	16	4058.48			

Df: Degrees of freedom; SS: Sum of squares; MS: Mean square.
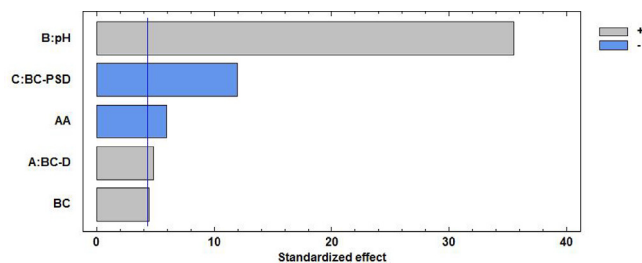

Fig. 5. Pareto chart representing the MG dye adsorption capacity by BWC. Operating conditions: $[MG]_0$ = 50 mg/L; BC-D = 6–12 g/L; solution pH = 4–10; BC-PSD = 225–525 μm; time = 5 min.
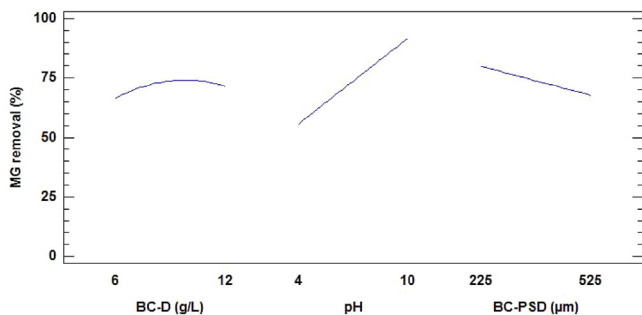

Fig. 6. Main effects representing the MG dye adsorption capacity by BWC. Operating conditions: $[MG]_0$ = 50 mg/L; BC-D = 6–12 g/L; solution pH = 4–10; BC-PSD = 225–525 μm; time = 5 min.

also achieved when microwave-induced NaOH activated carbon from biomass waste and H_2SO_4-treated Malaysian low rank coal were used for the removal of MB in water (Surip et al., 2020; Jawad et al., 2017). The elimination of other cationic dyes in aqueous matrices was also evaluated by Sewu et al. (2017) and found that high pH values were beneficial for this purpose (Sewu et al., 2017); while acidic conditions promoted the adsorption of anionic dyes (Wu et al., 2020).

In order to verify that the removal of MG was due to its retention on the BC surface instead of a structural change involving the color variation of the pollutant of interest, a control experiment was carried out. It is important to note that the color intensity of the MG probe dye is dependent on the solution pH since the structural properties vary as the solution pH is modified. Under this scenario, the color variation of a MG dye solution of 50 mg/L was assessed without adding BWC in a pH range between 4 and 10 through the measurement of the absorbance. After 5 min of residence time, the bluish-green color and its absorbance were found to be maintained throughout the pH range evaluated.

3.3.2. Effect of the BWC dose

As the BC-D is increased from 6 to 9 g/L, the MG dye uptake is also increased (Fig. 6). This can be ascribed to the rise in the number of effective sites at disposal for the retention of the tested dye (Jawad and Abdulhameed, 2020) and the larger surface area for the MG molecules uptake due to the number of pores is also increased. This effect has been reported in the literature for several pollutants contained in water and different adsorbing materials (Liu et al., 2020; Abukhadra et al., 2019). Nevertheless, as observed in Fig. 6, a further increment in the BC-D up to the central point of the studied range revealed a constant removal of the probe dye, with the subsequent reduction of the MG elimination capacity by the BC tested. This can be evidenced from the incipient curvature illustrated in the figure when a BC-D value close to 12 g/L is used. This phenomenon has been also informed previously and it can be ascribed to the excess of the BC dose, which is involved in the agglomeration of the BC particles within the solution, leading to the coverage of the BWC active sites and limiting the MG dye adsorption (Gokulan et al., 2019). In this case, the diffusion path length can be also increased, resulting in the desorption of some loose bonds (Marzbali et al., 2017). This effect was observed by Moosavi et al. (2020) when a nano-adsorbent derived from eggshell in the range from $0.01x10^{-1}$ to 0.20 g for the removal of acidic fuchsine (100 mg/L) and MG (100 mg/L) in water at a temperature of 26.85 °C was used.

This fact makes the BC-D used a parameter to be analyzed and optimized when evaluating the efficiency of an adsorbing agent in the treatment of polluted water.

3.3.3. Effect of the BWC particle size distribution

The BC-PSD is another factor to be considered when optimizing an adsorbing system since it was observed to play a significant role (p-value equal to 0.69×10^{-2}). In Fig. 6, the BC-PSD was evaluated within a range from 150 to 600 μm with average values at 225, 375 and 525 μm. It was found an increase in the BWC adsorption capacity as the PSD diminished.

It is important to highlight that the rise in the BC surface area is conferred by the distribution of the pores, and a larger surface area results in the adsorption of the pollutant of interest (Sizmur et al., 2017). The pollutant chemical adsorption by the functional groups contained on the BC surface and the electrostatic attraction between the pollutant ions in water and the BC surface are favored by the decrease in the size of the particles of the adsorbing material, since the number of pores and, therefore, the surface area ascribed to them are increased (Sizmur et al., 2017). In the adsorption study based on a BC derived from peanut shells for eliminating hexavalent chromium (Cr(VI)) in an aqueous solution, Han and coworkers (2016) observed a significant rise in the adsorption capacity of the tested BC as the PSD was reduced due to the increase in the surface area (Han et al., 2016).

A. Rubio-Clemente, J. Gutiérrez, H. Henao et al.

Furthermore, the interaction effect between the pH of the solution and the BC-PSD resulted to be significant with a positive influence in the adsorption system. This means that a higher removal percentage of the MG dye is achieved at a solution pH of 10 in comparison with the removal at a pH of 4, obtaining a more efficient adsorption system when a smaller BC-PSD is used, as illustrated in Fig. 7. The influence of the BC-PSD is more evident when the pH is 4. This can be explained as a consequence of the electrostatic repulsion forces between the MG dye cationic forms and the BC surface at acidic pH conditions.

3.4. Validation of the regression model and optimization of the adsorption system

From the ANOVA, a second-order regression model was constructed to represent the removal of MG by BWC. In Eq. (3), the quadratic regression model built is represented.

$$MG\ removal(\%) = 11.88 + 10.25x_1 + 3.90x_2 - 8.03 \times 10^{-2}x_3$$
$$- 5.24 \times 10^{-1}x_1^2 + 5.67 \times 10^{-3}x_2x_3 \quad (3)$$

The adequacy and suitability of the model was evaluated. The model was found to be significant (p-value = 0.00). Additionally, the percentage of the data variability explained by the model was measured through R^2 and R^2_{adj}. It was obtained that 94.54% and 92.06%, respectively, of the variability of the data is explained by the constructed regression model. Furthermore, the lack-of-fit test was conducted. As the p-value of this test was higher than 0.05 (0.10), it can be objectively assured that the built model fits well the observed data within the experimental domain.

Moreover, the regression model was validated for the assumptions of normality, independence and homoscedasticity. In Fig. 8, the normal probability plot is illustrated. It can be observed that the points are distributed throughout the straight line, with the exception of one point located at the upper right corner, which seems to be far from the straight line. Therefore, Shapiro–Wilk test was performed and the associated p-value (8.73×10^{-1}) confirmed that data are normally distributed. Homoscedasticity was also checked. As represented in Fig. 9, residuals do not follow any distribution pattern. In turn, Durbin-Watson test confirmed the independence of the data since the p-value obtained was higher than 0.05 (3.48×10^{-1}). Thus, the regression model can be used to represent the adsorption system for the removal of the MG dye contained in water by BWC.

The response surface associated with the constructed regression model was represented (Fig. 10) in order to locate from a graphical point of view the optimal operating conditions of the adsorbing system analyzed herein. It can be inferred that the highest MG removal within the experimental domain was obtained at the maximal pH and at the minimal BC-PSD tested. With regard to the BC-D, the maximal MG elimination was found to be near the central point of the range evaluated.

The response surface was used to estimate the operating conditions in terms of the BC dose and PSD, as well as the pH of the solution. It was found that the highest MG dye uptake by BWC (95.66%, with a desirability of 95.98%) was obtained at a solution pH of 10, a BC-PSD in the range from 150 to 300 μm, with a central point at 225 μm, and a BC-D of 9.80 g/L. In order to experimentally evaluate these results under optimal operating conditions, additional runs were executed and the MG removal (%) was registered.

As observed in Fig. 11, the MG dye removal was found to be 99.10% at 5 min of treatment. Once the equilibrium was reached, a MG elimination higher than 99.70% was achieved at 60 min. The MG elimination percentage was in the same order of magnitude as that one reported in the literature using a modified BC for the MG retention (Choudhary et al., 2020; Sharma et al.,
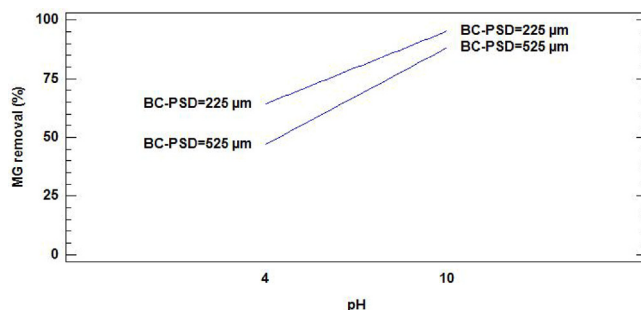

Fig. 7. Interaction effect between the pH of the solution and the BC-PSD. Operating conditions: [MG]$_0$ = 50 mg/L; BC-D = 6–12 g/L; solution pH = 4–10; BC-PSD = 225–525 μm; time = 5 min.
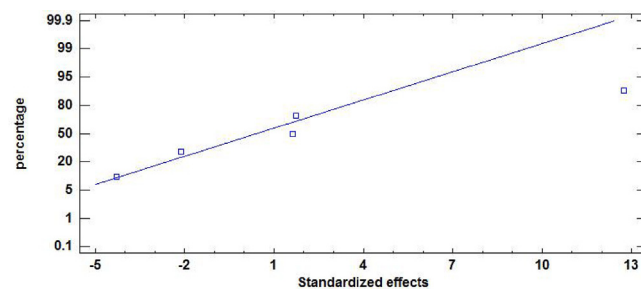

Fig. 8. Normal probability plot representing the MG dye adsorption capacity by BWC. Operating conditions: [MG]$_0$ = 50 mg/L; BC-D = 6–12 g/L; solution pH = 4–10; BC-PSD = 225–525 μm; time = 5 min.
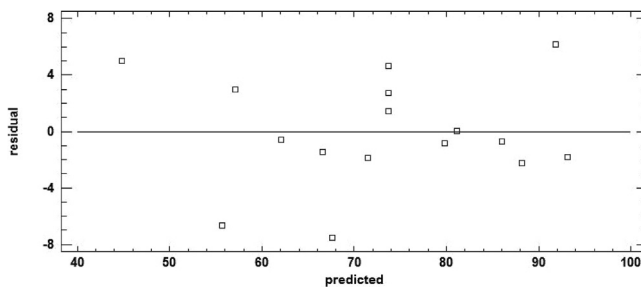

Fig. 9. Residuals vs. predicted values representing the MG dye adsorption capacity by BWC. Operating conditions: [MG]$_0$ = 50 mg/L; BC-D = 6–12 g/L; solution pH = 4–10; BC-PSD = 225–525 μm; time = 5 min.

2019). Similar results were also obtained for MB adsorption (Jawad et al., 2017, 2020; Jawad and Abdulhameed, 2020; Surip et al., 2020). In this regard, the use of the solid by-product generated from the micro-gasification of *Pinus patula* WC has been demonstrated to be efficient for the removal of dangerous pollutants such as MG in water.

4. Conclusions

Two BCs were prepared via micro-gasification of two biomass types (WP and WC) using a TLUD gasifier. The main operating conditions reached during the gasification process were an F$_r$ of 1.52 for WP and 1.85 for WC, the m$_{bms}$ ranged from 125.33 kg/h/m^2 for WP up to 145.39 kg/h/m^2 for WC; besides, the Y$_{char}$ values obtained for WP and WC were 12.12 wt%, and 10.82 wt%, respectively. The adsorption capacity of the tested BCs was initially evaluated for the removal of MG dye in an aqueous solution, considering the pH of the solution and the BC dose and PSD. The
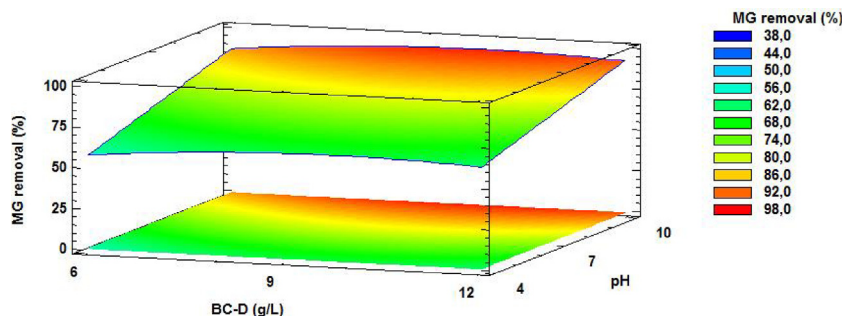
A. Rubio-Clemente, J. Gutiérrez, H. Henao et al.

Fig. 10. Response surface representing the MG dye adsorption capacity by BWC. Operating conditions: $[MG]_0$ = 50 mg/L; BC-D = 6–12 g/L; solution pH = 4–10; BC-PSD = 150–300 μm; time = 5 min.
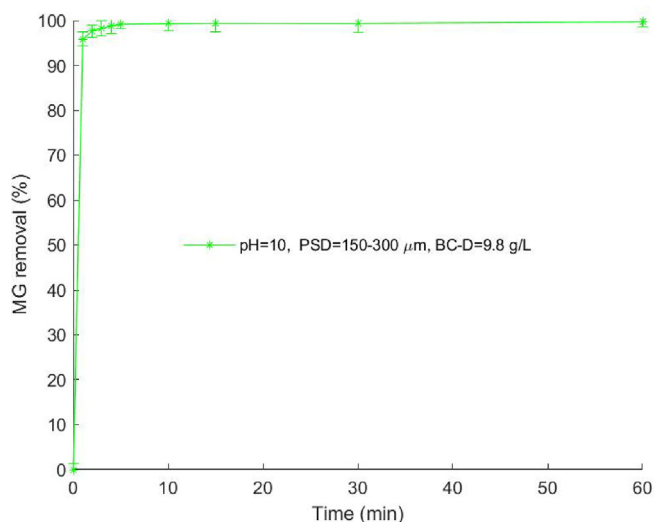

Fig. 11. MG adsorption vs. time by BWC. Operating conditions: $[MG]_0$ = 50 mg/L; pH = 10; BC-D = 9.80 g/L; BC-PSD = 150–300 μm; time = 60 min.

BC exhibiting the highest adsorption performance (85.90%) for a treatment time of 5 min under the experimental domain was BWC, which was selected for optimization purposes through the use of the RSM based on a face-centered CCD. The studied main factors were found to develop a significant role in the adsorption system, as well as the quadratic effect of the BC-D and the interaction effect between the solution pH and the PSD of the adsorbing material, since the p-values associated with these effects were lower than 0.05. For BWC, the optimal operating conditions regarding the pH of the water (10 pH units), the BC-PSD (150–300 μm) and the BC-D (9.80 g/L) resulted in a MG elimination higher than 99.70% at 60 min of contact time. The obtained second-order regression model, which was validated for normality, homoscedasticity and independency assumptions, was significant (p-value equal to 0.00) and fitted well the experimental data (R^2 and R^2_{adj} of 94.54% and 92.06%, respectively). The current study demonstrates that a waste obtained from the micro-gasification of *Pinus patula* WC can be used as an alternative material for treating highly toxic dyes contained in a real aqueous matrix. In this regard, new horizons are opened for the treatment of water pollution and the contribution to the sustainable development.

Declaration of Competing Interest

The authors declare that they have no known competing financial interests or personal relationships that could have appeared to influence the work reported in this paper.

Acknowledgement

References

Abukhadra, M.R., Sayed, M.A., Rabie, A.M., Ahmed, S.A., 2019. Surface decoration of diatomite by Ni/NiO nanoparticles as hybrid composite of enhanced adsorption properties for malachite green dye and hexavalent chromium. Colloids and Surfaces A: Physicochemical and Engineering Aspects 577, 583–593.

Bezerra, M.A., Ferreira, S.L.C., Novaes, C.G., Dos Santos, A.M.P., Valasques, G.S., da Mata Cerqueira, U.M.F., dos Santos Alves, J.P., 2019. Simultaneous optimization of multiple responses and its application in analytical chemistry–a review. Talanta 194, 941–959.

Choudhary, M., Kumar, R., Neogi, S., 2020. Activated biochar derived from opuntia ficus-indica for the efficient adsorption of malachite green dye, Cu^{+2} and Ni^{+2} from water. Journal of Hazardous Materials 392, 122441.

Díez, H.E., Pérez, J.F., 2019. Effects of wood biomass type and airflow rate on fuel and soil amendment properties of biochar produced in a top-lit updraft gasifier. Environmental Progress & Sustainable Energy 38, 13105.

de Farias, C.E., da Gama, B.M.V., da Silva Gonçalves, A.H., Medeiros, J.A., de Souza Abud, A.K., 2020. Basic-dye adsorption in albedo residue: effect of pH, contact time, dye concentration, biomass dosage, rotation and ionic strength. Journal of King Saud University-Engineering Sciences 32, 351–359.

Gokulan, R., Ganesh Prabhu, G., Jegan, J., 2019. A novel sorbent ulva lactuca-derived biochar for remediation of remazol brilliant orange 3R in packed column. Water Environment Research 91, 642–649.

González, W.A., Pérez, J.F., 2019. CFD analysis and characterization of biochar produced via fixed-bed gasification of fallen leaf pellets. Energy 186, 115904.

Gutiérrez, J., Rubio-Clemente, A., Pérez, J.F., 2021. Effect of main solid biomass commodities of patula pine on biochar properties produced under gasification conditions. Industrial Crops and Products 160, 113123.

Gwenzi, W., Chaukura, N., Noubactep, C., Mukome, F.N., 2017. Biochar-based water treatment systems as a potential low-cost and sustainable technology for clean water provision. Journal of Environmental Management 197, 732–749.

Hamad, H.T., 2021. Removal of phenol and inorganic metals from wastewater using activated ceramic. Journal of King Saud University-Engineering Sciences 33, 221–226.

Han, Y., Cao, X., Ouyang, X., Sohi, S.P., Chen, J., 2016. Adsorption kinetics of magnetic biochar derived from peanut hull on removal of Cr (VI) from aqueous solution: effects of production conditions and particle size. Chemosphere 145, 336–341.

Hubbard, W.G., 2015. Chapter 4 - wood bioenergy. In: Dahiya, A. (Ed.), Bioenergy. Academic Press, Boston, pp. 55–71.

Jawad, A.H., Abdulhameed, A.S., 2020. Statistical modeling of methylene blue dye adsorption by high surface area mesoporous activated carbon from bamboo chip using KOH-assisted thermal activation. Energy, Ecology and Environment 5, 456–469.

Jawad, A.H., Bardhan, M., Islam, M.A., Islam, M.A., Syed-Hassan, S.S.A., Surip, S., ALOthman, Z.A., Khan, M.R., 2020. Insights into the modeling, characterization and adsorption performance of mesoporous activated carbon from corn cob residue via microwave-assisted H3PO4 activation. Surfaces and Interfaces 21, 100688.

Jawad, A.H., Ishak, M.M., Farhan, A.M., Ismail, K., 2017. Response surface methodology approach for optimization of color removal and COD reduction of methylene blue using microwave-induced NaOH activated carbon from biomass waste. Water Treatment 62, 208–220.

Jindo, K., Mizumoto, H., Sawada, Y., Sanchez-Monedero, M.A., Sonoki, T., 2014. Physical and chemical characterization of biochars derived from different agricultural residues. Biogeosciences 11, 6613–6621.

A. Rubio-Clemente, J. Gutiérrez, H. Henao et al.

Kayan, B., Kalderis, D., Kulaksız, E., Gözmen, B., 2017. Adsorption of malachite green on fe-modified biochar: influencing factors and process optimization. Desalination Water Treatment 74, 383–394.

Kosek, K., Luczkiewicz, A., Fudala-Ksiżek, S., Jankowska, K., Szopińska, M., Svahn, O., Tränckner, J., Kaiser, A., Langas, V., Björklund, E., 2020. Implementation of advanced micropollutants removal technologies in wastewater treatment plants (wwtps)-examples and challenges based on selected eu countries. Environmental Science & Policy 112, 213–226..

Kurniawan, S., Yuliwati, E., Ariyanto, E., Morsin, M., Sanudin, R., Nafisah, S., et al., in press. Greywater treatment technologies for aquaculture safety. Journal of King Saud University-Engineering Sciences..

Lenis, Y., Pérez, J., 2014. Gasification of sawdust and wood chips in a fixed bed under autothermal and stable conditions. Energy Sources, Part A: Recovery, Utilization, and Environmental Effects 36, 2555–2565.

Liu, G., Abukhadra, M.R., El-Sherbeeny, A.M., Mostafa, A.M., Elmeligy, M.A., 2020. Insight into the photocatalytic properties of diatomite@ Ni/NiO composite for effective photo-degradation of malachite green dye and photo-reduction of Cr (VI) under visible light. Journal of Environmental Management 254, 109799.

Lou, K., Rajapaksha, A.U., Ok, Y.S., Chang, S.X., 2016. Pyrolysis temperature and steam activation effects on sorption of phosphate on pine sawdust biochars in aqueous solutions. Chemical Speciation & Bioavailability 28, 42–50.

Manojkumar, N., Muthukumaran, C., Sharmila, G., in press. A comprehensive review on the application of response surface methodology for optimization of biodiesel production using different oil sources. Journal of King Saud University-Engineering Sciences..

Marzbali, M.H., Mir, A.A., Pazoki, M., Pourjamshidian, R., Tabeshnia, M., 2017. Removal of direct yellow 12 from aqueous solution by adsorption onto spirulina algae as a high-efficiency adsorbent. Journal of Environmental Chemical Engineering 5, 1946–1956.

Medic, D., Darr, M., Potter, B., Shah, A., 2010. Effect of torrefaction process parameters on biomass feedstock upgrading. In: 2010 Pittsburgh, Pennsylvania, June 20-June 23, 2010. American Society of Agricultural and Biological Engineers, p. 1.

Mohamed, A., Ghobara, M.M., Abdelmaksoud, M., Mohamed, G.G., 2019. A novel and highly efficient photocatalytic degradation of malachite green dye via surface modified polyacrylonitrile nanofibers/biogenic silica composite nanofibers. Separation and Purification Technology 210, 935–942.

Montgomery, D.C., 2020. Introduction to Statistical Quality Control. John Wiley & Sons.

Moosavi, S., Li, R.Y.M., Lai, C.W., Yusof, Y., Gan, S., Akbarzadeh, O., Chowhury, Z.Z., Yue, X.G., Johan, M.R., 2020. Methylene blue dye photocatalytic degradation over synthesised Fe3O4/AC/TiO2 nano-catalyst: Degradation and reusability studies. Nanomaterials 10, 2360.

Nidheesh, P., Gopinath, A., Ranjith, N., Akre, A.P., Sreedharan, V., Kumar, M.S., 2020. Potential role of biochar in advanced oxidation processes: a sustainable approach. Chemical Engineering Journal 126582.

Pérez, J.F., Pelaez-Samaniego, M.R., Garcia-Perez, M., 2019. Torrefaction of fast-growing colombian wood species. Waste and Biomass Valorization 10, 1655–1667.

Protásio, T., Bufalino, L., Tonoli, G.H.D., Junior, M.G., Trugilho, P.F., Mendes, L.M., 2013. Brazilian lignocellulosic wastes for bioenergy production: characterization and comparison with fossil fuels. BioResources 8, 1166–1185.

Qian, K., Kumar, A., Patil, K., Bellmer, D., Wang, D., Yuan, W., Huhnke, R.L., 2013. Effects of biomass feedstocks and gasification conditions on the physiochemical properties of char. Energies 6, 3972–3986.

Rajabi, M., Mirza, B., Mahanpoor, K., Mirjalili, M., Najafi, F., Moradi, O., Sadegh, H., Shahryari-Ghoshekandi, R., Asif, M., Tyagi, I., et al., 2016. Adsorption of malachite green from aqueous solution by carboxylate group functionalized multi-walled carbon nanotubes: determination of equilibrium and kinetics parameters. Journal of Industrial and Engineering Chemistry 34, 130–138.

Rubio-Clemente, A., Chica, E., Peñuela, G.A., 2020. Photolysis of a mixture of anthracene and benzo[a]pyrene at ultra-trace levels in natural water with disinfection purposes. Journal of Environmental Sciences 92, 79–94.

Rubio-Clemente, A., Chica, E., Peñuela, G.A., 2021. Benzo[a]pyrene emerging micropollutant oxidation under the action of fenton reactants in real surface water: Process optimization and application. Polycyclic Aromatic Compounds 41, 95–108.

Sewu, D.D., Boakye, P., Jung, H., Woo, S.H., 2017. Synergistic dye adsorption by biochar from co-pyrolysis of spent mushroom substrate and saccharina japonica. Bioresource Technology 244, 1142–1149.

Sharma, G., Bhogal, S., Gupta, V.K., Agarwal, S., Kumar, A., Pathania, D., Mola, G.T., Stadler, F.J., 2019. Algal biochar reinforced trimetallic nanocomposite as adsorptional/photocatalyst for remediation of malachite green from aqueous medium. Journal of Molecular Liquids 275, 499–509.

Sizmur, T., Fresno, T., Akgül, G., Frost, H., Moreno-Jiménez, E., 2017. Biochar modification to enhance sorption of inorganics from water. Bioresource Technology 246, 34–47.

Stammati, A., Nebbia, C., De Angelis, I., Albo, A.G., Carletti, M., Rebecchi, C., Zampaglioni, F., Dacasto, M., 2005. Effects of malachite green (MG) and its major metabolite, leucomalachite green (LMG), in two human cell lines. Toxicology in Vitro 19, 853–858.

Surip, S., Abdulhameed, A.S., Garba, Z.N., Syed-Hassan, S.S.A., Ismail, K., Jawad, A.H., 2020. H2SO4-treated malaysian low rank coal for methylene blue dye decolourization and cod reduction: Optimization of adsorption and mechanism study. Surfaces and Interfaces 21, 100641.

Tkaczyk, A., Mitrowska, K., Posyniak, A., 2020. Synthetic organic dyes as contaminants of the aquatic environment and their implications for ecosystems: a review. Science of The Total Environment 717, 137222.

Tong, Y., McNamara, P.J., Mayer, B.K., 2019. Adsorption of organic micropollutants onto biochar: a review of relevant kinetics, mechanisms and equilibrium. Environmental Science: Water Research & Technology 5, 821–838.

Van Soest, P.v., Robertson, J., Lewis, B., 1991. Methods for dietary fiber, neutral detergent fiber, and nonstarch polysaccharides in relation to animal nutrition. Journal of Dairy Science 74, 3583–3597..

Vyavahare, G.D., Gurav, R.G., Jadhav, P.P., Patil, R.R., Aware, C.B., Jadhav, J.P., 2018. Response surface methodology optimization for sorption of malachite green dye on sugarcane bagasse biochar and evaluating the residual dye for phyto and cytogenotoxicity. Chemosphere 194, 306–315.

Wu, J., Yang, J., Feng, P., Huang, G., Xu, C., Lin, B., 2020. High-efficiency removal of dyes from wastewater by fully recycling litchi peel biochar. Chemosphere 246, 125734.

Zhang, A., Li, X., Xing, J., Xu, G., 2020. Adsorption of potentially toxic elements in water by modified biochar: A review. Journal of Environmental Chemical Engineering 104196.